

APPROVAL SHEET

Title of Thesis: Comparative study of receiver models for
optical communications systems

Name of Candidate: Anshul Kalra
Master of Science, 2006

Thesis and Abstract Approved: _____

Professor Curtis R. Menyuk
Computer Science and Electrical Engineering

Date Approved: _____

Curriculum Vitae

Anshul Kalra
26 Roberts St N, #514
Fargo, ND-58102
e-mail: anshul.kalra@ndsu.edu

Education

- M.S Electrical Engineering: Photonics
Thesis : Comparative study of receiver models for optical communications systems
University of Maryland, Baltimore County
- B.E Electronics
Thadomal Shahani Engineering College
Mumbai University, India

Employment

- August 2005-Present Teaching Assistant, Dept. of Mathematics
North Dakota State University, Fargo, ND.
- October 2001-July 2002 Trainee Engineer, Syntel(India) Ltd.
SEEPZ, Mumbai, India.

Publications

1. Anshul Kalra, John Zweck and Curtis Menyuk, "Comparison of bit-error rates for receiver models with integrate-and-dump and realistic electrical filters using the Gaussian approximation for pdfs", *in Proceedings of the Conference of Lasers and Electro-Optics (CLEO) 2004*, paper CWA24, San Francisco, CA, May 16-21, 2004.
2. Oleg V. Sinkin, Vladimir S. Grigoryan, Ronald Holzlöhner, Anshul

Kalra, John Zweck and Curtis R. Menyuk, "Calculation of error probability in WDM RZ systems in presence of bit-pattern-dependent nonlinearity and of noise", in *Proceedings of the Optical Fiber Communication Conference and Exposition (OFC) 2004*, paper TuN4, Los Angeles, CA, February 22-27, 2004.

Abstract

Title of Thesis: Comparative study of receiver models for optical communications systems

Anshul Kalra, Master of Science, 2006

Thesis directed by: Professor Curtis R. Menyuk
Computer Science and Electrical Engineering

The design and performance evaluation of optical fiber communications systems relies critically on receiver modeling. In this thesis, we compare two receiver models — the integrate-and-dump receiver and a realistic receiver using two current distributions to obtain the bit-error ratio (BER) from the two receiver models. The current distribution models used are the Gaussian approximation of the pdfs of the receiver current and the generalized χ^2 distribution of the pdfs of the receiver current.

Our results show that the BER obtained from the integrate-and-dump receiver model does not differ significantly from the BER obtained from the realistic receiver model.

**Comparative study of receiver models for
optical communications systems**

by
Anshul Kalra

Thesis submitted to the Faculty of the Graduate School
of the University of Maryland in partial fulfillment
of the requirements for the degree of
Master of Science

2006

© Copyright by Anshul Kalra, 2006

Acknowledgments

Most of all, I would like to thank my research advisor, Professor Curtis R. Menyuk, whose guidance, stimulating suggestions, and constructive criticism helped me in both my research and the writing of this thesis.

I am also deeply indebted to Professor John Zweck for his valuable advice and friendly help. Extensive discussions with him and detailed suggestions for my work have played an important part in the development of this study.

Thanks also goes to my colleagues for whom I have great regard and from whom I have learned a large amount. Specifically, I want to thank Dr. Brian Marks, Dr. Ivan Lima, Dr. Ronald Holzlohner, Oleg Sinkin, and Jonathan Hu.

I express my thanks and appreciation to my family for their understanding, motivation, and patience. Lastly, but in no sense least, I am thankful to all my colleagues and friends who made my stay at UMBC a memorable and valuable experience.

Table of Contents

List of Figures	v
1 Introduction	1
2 Receiver — An overview	6
2.1 Optical communication systems	6
2.2 Basic receiver design	8
2.2.1 Integrate-and-dump receiver model	10
2.2.2 Realistic receiver model with practical filters	12
2.3 Noise in optical communication systems	15
2.3.1 Optical noise	15
2.3.2 Electronic noise	17
2.3.3 Noise covariance matrix	18
2.4 System performance metrics	19
3 Assumed current distributions	22
3.1 Gaussian current distribution	22
3.2 χ^2 current distribution	25
3.3 Algorithm	31

4	Results	33
4.1	Effect of varying electrical filter bandwidth	34
4.2	Effect of varying signal rise time	39
4.3	Effect of varying OSNR	41
5	Conclusion	43

List of Figures

1.1	Schematic illustration of the receiver models and assumed current distributions. We investigate all four combinations. The receiver models differ in their treatment of the optical and electrical filters. The assumed current distribution applies at the detection point at the end of the receiver models. The Gaussian probability distribution is a commonly used approximation while the generalized χ^2 probability distribution model is exact for the receiver models that we are considering.	5
2.1	Schematic illustration of a basic receiver	8
2.2	Comparison of the power transfer function for a three-mirror Fabry Perot(—) and a two-mirror Fabry Perot(- -)filter. . . .	13

4.1	RZ pulse format. BER as a function of the electrical filter bandwidth. The BER variations for a realistic receiver model using a Gaussian current distribution and a χ^2 current distribution are shown by dashed and solid curves, respectively. The results for the integrate-and-dump receiver model using a Gaussian current distribution and a χ^2 current distribution are shown by straight lines, marked by circles and squares respectively.	35
4.2	RZ pulse format. Decision threshold as a function of the electrical filter bandwidth. The decision threshold variations for a realistic receiver model using a Gaussian current distribution and a χ^2 current distribution are shown by dashed and solid curves, respectively. The results for the integrate-and-dump receiver model using a Gaussian current distribution and a χ^2 current distribution are shown by straight lines, marked by circles and squares respectively.	36
4.3	NRZ pulse format. BER as a function of the electrical filter bandwidth. The BER variations for a realistic receiver model using a Gaussian current distribution and a χ^2 current distribution are shown by dashed and solid curves, respectively. The results for the integrate-and-dump receiver model using a Gaussian current distribution and a χ^2 current distribution are shown by straight lines, marked by circles and squares respectively.	37

4.4	Decision threshold as a function of the electrical filter bandwidth for the NRZ pulse format. The decision threshold variations for a realistic receiver model using a Gaussian current distribution and a χ^2 current distribution are shown by dashed and solid curves, respectively. The results for the integrate-and-dump receiver model using a Gaussian current distribution and a χ^2 current distribution are shown by straight lines, marked by circles and squares respectively.	38
4.5	Variation of the BER with a change in rise time of the NRZ pulse. The results for the realistic receiver model using a Gaussian current distribution and a χ^2 current distribution are shown by dashed and solid lines, respectively. The results for the integrate-and-dump receiver model using a Gaussian current distribution and a χ^2 current distribution are shown by the dotted lines, marked by circles and squares respectively.	39
4.6	Variation of decision voltage with change in rise time of the NRZ pulse. The results for the realistic receiver model using a Gaussian current distribution and a χ^2 current distribution are shown by dashed and solid lines, respectively. The results for the integrate-and-dump receiver model using a Gaussian current distribution and a χ^2 current distribution are shown by the dotted lines, marked by circles and squares respectively.	40

4.7	Variation of the BER versus OSNR for the RZ modulation format. The BER variations for the realistic receiver model using a Gaussian current distribution and a χ^2 current distribution are shown by dashed and solid curves, respectively. The results for the integrate-and-dump receiver model using a Gaussian current distribution and a χ^2 current distribution are shown by dotted lines, marked by circles and squares respectively. . .	41
4.8	Variation of the decision voltage versus OSNR for the RZ modulation format. The decision threshold variations for the realistic receiver model using a Gaussian current distribution and a χ^2 current distribution are shown by dashed and solid curves, respectively. The results for the integrate-and-dump receiver model using a Gaussian current distribution and a χ^2 current distribution are shown by dotted lines, marked by circles and squares respectively.	42

Chapter 1

Introduction

The invention of the laser and the development of optical fibers that are able to carry light signals over long distances have resulted in the development of high-speed optical telecommunications systems. The laying of undersea long-haul fiber cables connecting the different continents in the 1980's and 90's resulted in cheaper long distance communications. The "Internet Revolution" that we are experiencing today would not have been possible without the extensive deployment of high-data-rate optical fiber transmission systems during the last two decades. The growing use of optical fibers has also meant that larger bandwidths are available for communications applications, thus providing an impetus for the development and implementation of better technologies in networking, signal processing, and communications software and hardware [1].

Optical fibers offer several advantages over other signal transmission media like radio, satellites, coaxial cable, or the traditional copper wire. Fiber optic cables can support much higher data rates, and they are less lossy,

so that they have the ability to carry information signals over much longer distances.

The pressing demand for more bandwidth in today's world, primarily due to the evolution of the internet and high speed computer networks, has resulted in a requirement for the design of better optical communications systems that can support even higher data rates and are more reliable.

As optical communications systems have become faster and more complex, computational modeling has become an important tool in the evaluation and design of these systems and their components. The necessity for fast modeling tools, coupled with the complexity of optical transmission systems, makes it necessary to use a number of approximations and assumptions in modeling.

Often, engineers and physicists are only interested in understanding issues related to the transmission of signals. Alternatively, they may only be interested in understanding issues related to the receiver. Hence, a general practice is to separate the transmission modeling from the receiver modeling. Highly simplified models are often used for the transmission or the receiver or both. It is rare that both the transmission and the receiver are accurately modeled in a simulation.

However, one must carefully analyze and understand the limitations of making simplifying assumptions and approximations by comparison with more rigorous and detailed models. For example, a commonly used simplification in receiver modeling is to assume a Gaussian distribution for the probability density functions (pdfs) of the current in the receiver. The degree of validity of this assumption has been discussed in papers written by Lee and Shim [2] and Forestieri [3] who demonstrated that the current distribution of

the marks and of the spaces in the receiver is a generalized χ^2 distribution and that the Gaussian approximation overestimates the minimum bit-error ratio (BER) by one to two orders of magnitude.

Another common simplification for the receiver is to model the electrical filtering as an integrate-and-dump operation. This approximation makes calculating the distribution of the current in the receiver easier than when using an accurate filter model, and in certain cases yields analytical expressions for the BER and Q -factor [4], [5]. In a previously published work, my colleagues and I compared receiver models with integrate-and-dump and realistic electric filters using the Gaussian approximation of the voltage pdfs. We showed that the BERs are comparable, but the decision thresholds differ significantly [6].

This thesis addresses the issue of the validity of the integrate-and-dump receiver approximation. My colleagues and I made an in-depth comparison between the integrate-and-dump receiver model — which consists of a pass-band optical filter, a square-law detector, and an integrate-and-dump electrical filter — with a realistic receiver model that has practically realizable optical and electrical filters. The performance of the two receiver models is quantified by comparing the calculated BERs.

When comparing the receiver models, we used two current distributions for each of them when computing the BER. The first current distribution is the commonly-used Gaussian approximation of the pdfs of the receiver current. The second current distribution uses the real pdfs of the receiver current. These pdfs obey a generalized χ^2 distribution. We then computed the BER from these pdfs. We compared the BERs and the corresponding

decision thresholds for the two receiver models, using these two current distributions. Please refer to Figure 1.1 on page 5 for a schematic elaboration of the work proposed in this thesis.

Although I show results for all four combinations, the following comparisons are the most relevant and I will focus on these.

1. The comparison between the integrate-and-dump receiver model with a current distribution employing the Gaussian approximation of the pdfs and the realistic receiver model with a current distribution using the generalized χ^2 pdfs.
2. A comparison between the integrate-and-dump receiver model and the realistic receiver model with a current distribution using the generalized χ^2 pdfs.

A thorough comparison between the two receiver models is made by looking at how closely the BERs and decision thresholds match for various signal modulation formats, filter bandwidths, noise power levels, and extinction ratios. The signal modulation formats used are return-to-zero (RZ) and non-return-to-zero (NRZ). The impact of changing the pulse duration for RZ pulses and the rise time for NRZ pulses is also studied.

The outline of the thesis is as follows: Chapter 2 briefly describes optical fiber communications systems and in particular discusses receivers for these systems. I also discuss in detail the design of the integrate-and-dump receiver model and the realistic receiver model. Chapter 3 contains the theory of the two current distributions that we used — the Gaussian approximation of the pdfs and the generalized χ^2 pdfs. The generalized χ^2 pdfs are exact, assum-

ing square-law detection and linear electrical filtering. The C++ algorithm used to simulate and compare the two receiver models with the two assumed current distributions is also illustrated in this chapter. The simulation results are presented in Chapter 4. I summarize the results of my thesis and draw my main conclusions in Chapter 5.

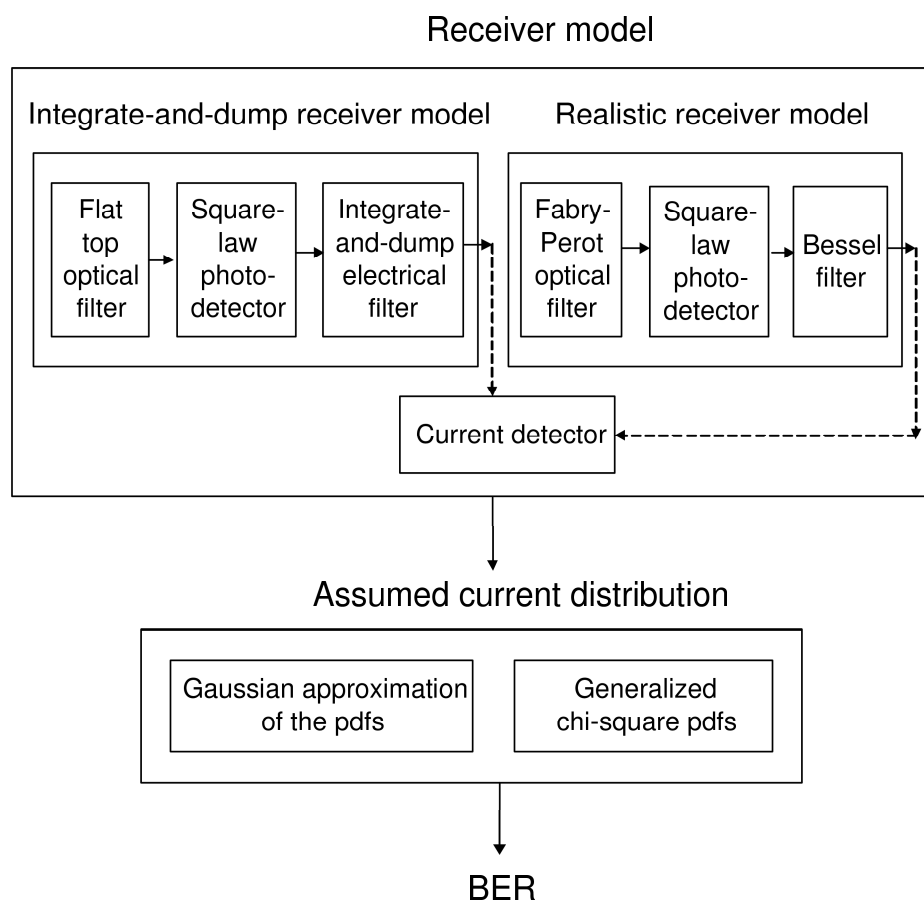


Figure 1.1: Schematic illustration of the receiver models and assumed current distributions. We investigate all four combinations. The receiver models differ in their treatment of the optical and electrical filters. The assumed current distribution applies at the detection point at the end of the receiver models. The Gaussian probability distribution is a commonly used approximation while the generalized χ^2 probability distribution model is exact for the receiver models that we are considering.

Chapter 2

Receiver — An overview

This chapter provides a description of the receivers in modern optical fiber communications systems. I start with a brief description of a simplified optical communications system in Section 2.1. Section 2.2 provides a schematic description of a basic receiver design and describes in detail the integrate-and-dump receiver model and the realistic receiver model with practical filters. Section 2.3 deals with noise — optical noise that is generated during transmission and both optical and electrical noise that is generated in the receivers. In Section 2.4, I review some of the commonly-used measures of system performance in optical fiber communications systems.

2.1 Optical communication systems

An optical fiber communications system consists of a transmitter, a transmission line, and a receiver. Typically, the transmitter consists of a laser diode and a modulator, the transmission line consists of a chain of cascaded optical

fibers and optical amplifiers, and the receiver consists of a photodetector, optical and electrical filters, amplifiers, and a decision circuit.

Optical signal transmission in fibers is impaired by signal distortion, signal loss, and noise. The impairments can be attributed to effects such as chromatic dispersion and the Kerr nonlinearity, which cause temporal broadening and spectral broadening of the optical pulse, respectively. The combined effects of these two phenomena on pulse evolution are in general complicated. Signal distortion is also introduced by the interaction between neighboring signal pulses in the same wavelength channel and crosstalk between adjacent channels. Random fluctuations in the fiber birefringence give rise to polarization-mode dispersion (PMD), which causes further degradation by broadening the pulse. Optical amplifiers are used to overcome the signal loss along the fiber. Their drawback is that they introduce amplified spontaneous emission (ASE) noise [7].

Due in part to the large number of complex components making up an optical transmission system and the various transmission impairments just described, modeling optical transmission systems is complicated. One way to gain insight into system performance in the presence of noise or other statistical impairments is by using Monte-Carlo techniques [8]. However, Monte-Carlo techniques are computationally expensive, and the accuracy of the results grows typically only as the square root of the number of system realizations. The computational time required for these simulations may be prohibitively large. Thus, it is often useful to make simplification that will allow the modeler to calculate the pdf of the noise or some other fluctuation analytically or through a simple computation. For example, it is very common

to assume that the noise is unaffected by the transmission and is determined by the gain profiles and the spontaneous emission factors of the amplifiers in the transmission line. In this case, the noise pdf can be found analytically [4].

Transmission modeling can often be separated from receiver modeling, especially when one is solely interested in analyzing transmission problems. The same is true for modeling receivers. The performance and design of receivers can be understood without considering transmission effects. In order to compare the two receiver models — the integrate-and-dump receiver model and the realistic receiver model — my colleagues and I have neglected all transmission effects. The inputs to the receiver model are the noise-free signal and noise that is additive, white, and Gaussian. The additive white Gaussian noise (AWGN) assumption for the input to the optical receiver often works well in practice [9].

2.2 Basic receiver design

In this thesis, we are concerned with the design of receivers for the amplitude-shift keyed (ASK) modulation format only. The basic receiver design that will

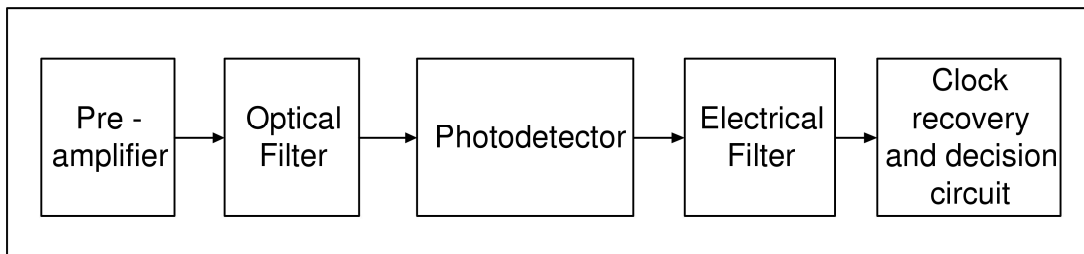


Figure 2.1: Schematic illustration of a basic receiver

be studied in this thesis is shown in Fig. 2.1. Modern commercial receivers are

more complicated than the design in Fig. 2.1, and the details of their designs are usually proprietary and thus not generally available. However, the simple receiver design illustrated in Fig. 2.1 is adequate to describe the essential signal processing that occurs in the receiver. This design is often studied in the scientific literature [1]. Moreover, this receiver approximates well the receiver design for the experiments that are carried out at UMBC [10].

A pre-amplifier is first used to boost the received signal power to a level at which the optical noise will dominate over the electrical noise in the receiver. Previous studies have shown that optical pre-amplification increases receiver sensitivity [11]. The pre-amplifier also adds noise to the signal, which can be approximated as AWGN.

The optical filters generally used in optical communication systems are either Fabry-Perot interferometers, Bragg gratings or array waveguide gratings (AWG). The function of the optical filter is to demultiplex channels and to limit the amount of noise entering the photodetector. In this thesis, I have computationally implemented a passband filter and a three-mirror Fabry-Perot filter for modeling the optical filter in the integrate-and-dump receiver model and the realistic receiver model, respectively.

The photodetector converts the optical signal into an electrical signal. A simple model of the photodetector that neglects shot noise and dark current can be described by the equation $I_{\text{out}} = \kappa |E_{\text{in}}|^2$. The input to the photodetector is E_{in} , which is the sum of the electrical field envelopes of the optical signal and noise, and I_{out} is the output current. The parameter κ is the responsivity of the photodetector. The photodetector squares the combined signal and noise, which results in noise-noise beating and signal-noise beating

contributions to the photodetector current, so that

$$\begin{aligned} I_{\text{out}} &= \kappa |e_{\text{in}} + \delta e_{\text{noise}}|^2 \\ &= \kappa [|e_{\text{in}}|^2 + |\delta e_{\text{noise}}|^2 + e_{\text{in}} \delta e_{\text{noise}}^* + e_{\text{in}}^* \delta e_{\text{noise}}], \end{aligned} \quad (2.1)$$

where e_{in} is the noise-free electrical field envelope and δe_{noise} is the noise contribution to the electrical field envelope entering the photodetector.

I emphasise that photodetection is a nonlinear process. This operation is the only nonlinear operation in our receiver model and is the reason that the exact current pdf does not obey a multivariate Gaussian distribution.

After photodetection, electrical filtering is done to remove noise. The design of the electrical filter crucially affects the receiver performance. The BER increases significantly if one chooses a bandwidth that is too large or too small. We define the bandwidth of the electrical filter as the frequency separation between the 3-dB points of the filter, which are the points corresponding to a reduction of signal power by 50% relative to the peak. In the realistic receiver model, I model the electrical filter as a Bessel filter. All optical and electrical filters discussed in this thesis have been modeled as lossless devices at the peak, *i.e.*, $H(\omega = 0) = 1.0$, where $H(\omega)$ is the frequency response of the filter.

2.2.1 Integrate-and-dump receiver model

The integrate-and-dump receiver model consists of a preamplifier, a passband optical filter, a square-law detector, and an integrate-and-dump electrical filter. The chief advantage of this model is that it simplifies the mathematics

of the receiver model. Neglecting transmission effects and assuming that the optical noise entering the receiver is AWGN, Marcuse [4] and Humblet and Azizoglu [5] have shown that the pdf of the current in the receiver for both the marks (1's) and the spaces (0's) can be expressed in terms of elementary functions and Bessel functions.

Integrate-and-dump filter

The integrate-and-dump filter processes an input signal just as the name suggests; it finds the total current in a bit period and at the end of the bit period, it “dumps” out the average current in the bit period:

$$I_{\text{out}}(t) = \frac{1}{T} \int_{t-T}^t I_{\text{in}}(t) dt, \quad (2.2)$$

where T is the bit period.

This filter is close to ideal for digital optical communication systems, since it integrates all the current inside a bit slot and none of the current outside, thus minimizing interference between neighboring bits. However, it is physically unrealizable.

Since filters are generally described in the frequency domain, we will next use equation (2.2) to calculate the frequency response of an integrate-and-dump filter. Filtering in the time domain is equivalent to a convolution between the signal and the filter function. Hence, we can write $y(t) = \int_{-\infty}^{\infty} h(\tau)x(t - \tau)d\tau$, where $x(t)$ is the input signal, $h(t)$ is the filter function in the time domain, and $y(t)$ is the filtered current. In the time domain,

the integrate-and-dump operation is a gating function,

$$\begin{aligned} h(t) &= \frac{1}{T}, & 0 < t < T \\ &= 0, & \text{otherwise} \end{aligned} \quad (2.3)$$

The filter function in the frequency domain can then be found by taking the Fourier transform:

$$H(\omega) = \int_{-\infty}^{\infty} h(t)\exp(i\omega t)dt = \frac{\exp(i\omega T) - 1}{i\omega T}. \quad (2.4)$$

2.2.2 Realistic receiver model with practical filters

In the realistic receiver model that my colleagues and I have used to make a performance comparison with the integrate-and-dump receiver model, the optical filter is a three-mirror Fabry-Perot filter and the electrical filter is a fifth-order Bessel filter.

Fabry-Perot filter

A single-cavity, two-mirror Fabry-Perot interferometer makes use of multiple reflections between two closely spaced, partially-silvered surfaces. The frequency response of the filter can be changed by changing the air pressure between the two mirrors, or by changing the spacing between the two mirrors, or by varying the tilt of the mirrors. A three-mirror Fabry-Perot filter performs better than a two-mirror Fabry-Perot filter [12]. Figure 2.2 compares the performance of a three-mirror Fabry-Perot filter with that of a two-mirror

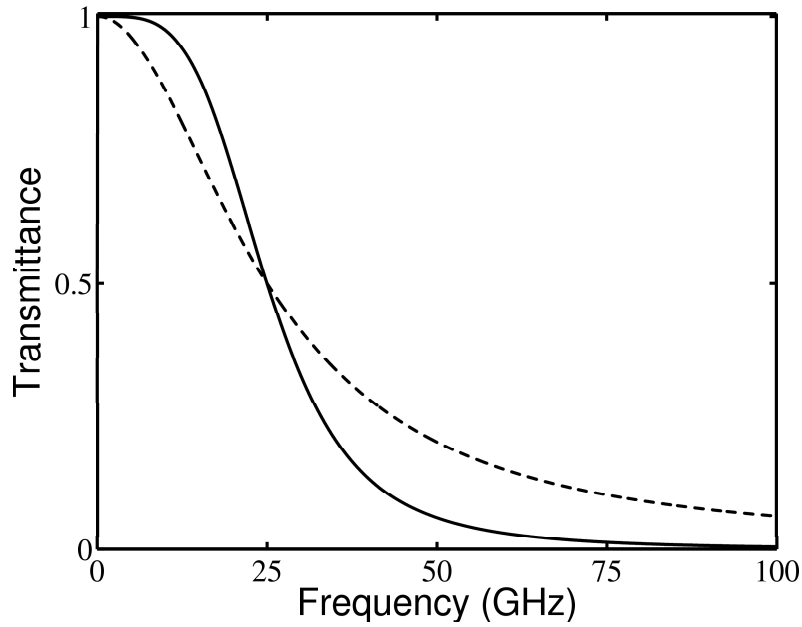


Figure 2.2: Comparison of the power transfer function for a three-mirror Fabry Perot(—) and a two-mirror Fabry Perot(- -)filter.

Fabry-Perot filter, both having the same half-width half maximum (HWHM) bandwidth of 25 GHz. Since the three-mirror Fabry-Perot response is more flat-topped and then it dies more quickly, it gives a superior performance compared to the two-mirror Fabry Perot filter. Assuming that there are no losses, the frequency response of a three-mirror Fabry-Perot filter [13] is given by

$$H(\omega) = \frac{\sqrt{T_0 T_1}}{1 - 2\sqrt{R_0 R_1} \exp(i\omega/\text{FSR}) + R_1 \exp(2i\omega/\text{FSR})}, \quad (2.5)$$

where R_0 and R_1 are the reflectances, while T_0 and T_1 are the transmittances of the center and the outer mirrors respectively. The factor FSR is the free spectral range of the cavity. The frequency response of the filter is of the

second-order Butterworth type [12] if one sets the value of R_0 to

$$R_0 = \frac{4R_1}{(1 + R_1)^2}. \quad (2.6)$$

My colleagues and I have set R_1 equal to 0.8. This value is typical in practice [12]. The power spectral width B_0 is a useful measure of the optical filter bandwidth, which we define as

$$B_0 = \int_{-\infty}^{\infty} |H(f)|^2 df, \quad (2.7)$$

where $H(f)$ is normalized so that $H(0) = 1$ and $H(f)$ is unitless.

Bessel filter

The Bessel filter's distinguishing characteristic is the near-constant group delay throughout the pass band of the low-pass filter [14]. The phase response of a Bessel filter has a slower rate of change than in the case of a Butterworth or a Chebyshev filter. Hence, if a waveform with high harmonic content is filtered, such as a square wave, the delay in the harmonics relative to the fundamental frequency is smaller for a Bessel filter than it is for a Butterworth or a Chebyshev filter, so that there is less overshoot and ringing of the signal. Its disadvantage is that it has a slower initial rate of attenuation beyond the passband than does a Butterworth filter. It takes a higher-order Bessel filter to give a magnitude response similar to a given Butterworth filter, but the pulse fidelity of the Bessel filter makes the added complexity worthwhile in practice. The Bessel filter can be implemented as a ladder of capacitors and

inductors. The frequency response of a fifth-order Bessel filter is given as

$$H(s) = \frac{945}{s^5 + 15s^4 + 105s^3 + 420s^2 + 945s + 945}, \quad (2.8)$$

where $s = -i\alpha f/f_{3\text{db}}$, where $f_{3\text{db}}$ is the 3 dB filter bandwidth and α is a scaling factor. For a fifth-order Bessel filter α equals 2.4274.

2.3 Noise in optical communication systems

Noise in optical fiber communication systems is added in both the optical fiber transmission line and in the receiver. The noise added during transmission is due to ASE noise from the amplifiers. The receiver adds noise in the optical domain from the pre-amplifier prior to photodetection and in the electrical domain after photodetection. Receiver sensitivity is highest when optical noise from the pre-amplifier is greater than the receiver's electrical noise [11].

2.3.1 Optical noise

Both thermal noise and amplified spontaneous emission (ASE) noise contribute in principle to optical noise during transmission; however, thermal noise power is completely negligible. ASE noise from erbium-doped fiber amplifiers (EDFAs) is due to spontaneous transitions in which erbium ions randomly make a transition to a lower energy state and emit a photon. As a consequence of the noise, there is a minimum threshold for the transmitted signal power below which a mark cannot be distinguished from a space by the decision circuitry with an acceptable BER. ASE noise is also responsible for

partial saturation of the optical amplifiers located further down the fiber link, which may result in reduced signal gain from the amplifier [7]. Heffner [15] showed that the minimum added noise power P_N is equal to

$$P_N = h\nu B(G - 1), \quad (2.9)$$

where G is the amplifier gain, B is the full width half maximum (FWHM) bandwidth, h is Planck's constant, and ν is the frequency of light corresponding to the center wavelength of the light signal. Equation (2.9) represents the quantum limit. Modern amplifiers exceed this limit by a factor referred to as the spontaneous emission factor n_{sp} , which is usually less than two.

Each amplifier adds noise to the signal independently. To determine the noise at the receiver when the nonlinear interaction between the signal and the noise can be neglected, one may simply sum the noise from all the in-line amplifiers. I quantify the noise power using the noise spectral density, N_{ASE} , which is defined as

$$N_{ASE} = \frac{P_{N-total}}{B_{OSA}}, \quad (2.10)$$

where $P_{N-total}$ is the total noise power due to all the in-line amplifiers in the transmission line and the pre-amplifier of the receiver, B_{OSA} is the power equivalent spectral width of the optical spectrum analyzer (OSA) and is given by $B_{OSA} = \int_{-\infty}^{\infty} |h_{OSA}(\tau)|^2 d\tau$, where $h_{OSA}(\tau)$ is the impulse response of the OSA. The OSA is placed at the receiver and its frequency window is set equal to 25 GHz. The OSA is used by experimentalists to find the optical signal to noise ratio (OSNR) in a frequency window. Neglecting all transmission effects implies that the optical signal power remains unchanged and that the

noise power can be calculated from the SNR value determined from the OSA.

By modeling the noise entering the receiver as AWGN, I have neglected signal-noise interactions and noise-noise interactions during transmission. Considering signal-noise interaction during transmission would result in multivariate-Gaussian-distributed noise at the input to the receiver. We make the AWGN assumption for the following reasons:

1. For a number of optical communication systems, nonlinearity is quantitatively a small effect and the resulting signal-noise interactions are weak. For such systems, AWGN noise at the input of the receiver is sufficient to describe the noise characteristics of the system.
2. Since the goal of this thesis is to compare different receiver models, it is both sensible and standard to take the simplest possible model for transmission noise.

2.3.2 Electronic noise

Any part of the receiver containing a resistive element can give rise to *thermal* or *Johnson* noise [1], [9]. This noise is associated with the random thermal motion of charge carriers in the dissipative element. In the case of an optical communication system receiver, this noise is primarily added by the load resistor in the receiver input circuit. Thermal noise can be considered white noise for all practical purposes.

Shot noise is noise caused by current fluctuations, which are due to the discreteness of charge carriers [9]. The noise spectral density of shot noise is independent of frequency and hence is white. Dark current noise and

quantum noise are two types of noise that manifest themselves as shot noise. Dark current noise results from dark current that continues to flow in the photodiode when there is no incident light. Dark current noise is independent of the optical signal. In addition, the discrete nature of the photodetection process creates a signal-dependent shot noise called quantum noise. Quantum noise results from the random generation of electrons by the incident optical radiation.

In modern optical communication systems, the contributions of electrical noise are negligible when compared to optical ASE noise, and hence we neglect the electronic noise sources.

2.3.3 Noise covariance matrix

To describe the statistics of noise evolution in an optical fiber transmission system, we expand the noise signal as a Fourier series. The noise evolution in an optical fiber transmission line can be described by utilizing a covariance matrix. An individual element of the covariance matrix $K_{ij} = \text{cov}(x_i, x_j)$ is given by,

$$\text{cov}(x_i, x_j) = \langle (x_i - \mu_i)(x_j - \mu_j) \rangle = \langle x_i x_j \rangle - \langle x_i \rangle \langle x_j \rangle. \quad (2.11)$$

The two variates, x_i and x_j are the Fourier coefficients of the noise signal and $\mu_i = \langle x_i \rangle$ and $\mu_j = \langle x_j \rangle$ are the means of x_i and x_j respectively. When $i = j$, we obtain

$$\text{cov}(x_i, x_i) = \langle x_i^2 \rangle - \langle x_i \rangle^2 = \sigma^2. \quad (2.12)$$

With no transmission effects, the noise signal remains white. In this case, the Fourier coefficients of the noise signal are independent and identically-distributed Gaussian variables with zero mean and with a variance σ^2 that is equal to the noise power in the frequency band occupied by one Fourier component. Since the covariance of two independent variables is zero, the noise covariance matrix at the input of the receiver is a diagonal matrix and each diagonal element equals σ^2 .

The power of the noise signal, P_N , can be written as

$$P_N = N_{\text{ASE}}\Delta f N, \quad (2.13)$$

where N_{ASE} is the noise spectral density, Δf is the frequency window occupied by one Fourier component, and N is the number of frequencies in the discrete-time Fourier transform (DTFT) of the signal. The relation between the noise spectral density and the diagonal element K_{ii} of the covariance matrix is $N_{\text{ASE}} = \sigma^2/\Delta f$.

2.4 System performance metrics

The most fundamental measure of system performance is the bit error ratio (BER). It is defined as the ratio of the total number of received bits in error to the total number of bits transmitted. Assuming that the likelihood of transmission of a mark is the same as that of a space, the BER can be expressed as

$$\text{BER}(y_d) = \frac{1}{2}[P_{0|1}(y_d) + P_{1|0}(y_d)], \quad (2.14)$$

where $P_{0|1}(y_d)$ is the probability of receiving a space when a mark is transmitted when y_d is the decision threshold. Analogously $P_{1|0}(y_d)$ is the probability of detecting a mark when a space is transmitted, where y_d is the decision level. These two probabilities are defined as

$$P_{0|1}(y_d) = \int_0^{y_d} f_{y1}(y)dy, \quad (2.15)$$

$$P_{1|0}(y_d) = \int_{y_d}^{\infty} f_{y0}(y)dy, \quad (2.16)$$

where f_{y1} and f_{y0} are the pdfs of the received low-pass filtered electrical current in the marks and in the spaces, respectively. These pdfs are dependent on the sampling time at the receiver.

Accurate computation of the BER for even approximate system models can be difficult. A commonly used approach to obtain an estimate of this quantity is to approximate the pdfs of the current at the decision point in the receiver by assuming that they are Gaussian-distributed. With Gaussian pdfs for the marks and spaces, one finds that [16]

$$\text{BER}(y_d) = \frac{1}{4} \left[\text{erfc} \left(\frac{\mu_1 - y_d}{\sqrt{2}\sigma_1} \right) + \text{erfc} \left(\frac{y_d - \mu_0}{\sqrt{2}\sigma_0} \right) \right], \quad (2.17)$$

where μ_0 , μ_1 are the mean values, σ_0 , σ_1 are the standard deviations of the current in the spaces and the marks respectively, and erfc is the complement of the error function. The decision level corresponding to the minimum BER can be obtained by setting the derivative of Equation (2.17) with respect to y_d equal to zero.

Another widely-used performance measure is the Q -factor. It can be

obtained from Equation (2.17) by setting the probability of error in the marks and the spaces equal, so that

$$\begin{aligned} Q &= \frac{\mu_1 - y_d}{\sigma_1} = \frac{y_d - \mu_0}{\sigma_0} \\ &= \frac{\mu_1 - \mu_0}{\sigma_1 + \sigma_0}. \end{aligned} \quad (2.18)$$

In the Gaussian approximation of the pdfs of the current in the marks and spaces, the relationship between the BER and the Q -factor is

$$\text{BER} = \frac{1}{2} \text{erfc} \left(\frac{Q}{\sqrt{2}} \right). \quad (2.19)$$

Although the value of BER obtained from Q is not the minimum BER that can be obtained from equation (2.17), it becomes equal to it when Q is large and is close to it for practical Q values [16].

Another important figure of merit that is even easier to measure is the OSNR (optical signal-to-noise ratio). It measures the ratio of optical signal power to noise power for a specified optical bandwidth. It is generally measured before the receiver by using an optical spectrum analyzer (OSA).

From the definition of OSNR, we have $\text{OSNR} = P_S/P_N$, where P_S is the signal power and P_N is the noise power, at the input of the receiver. We use the results from Subsection 2.3.3 to show that the OSNR is related to the variance $\sigma^2 = K_{ii}$ by

$$\text{OSNR} = \frac{P_S}{(K_{ii})N} \quad (2.20)$$

In our simulations, the OSNR is used to characterize the statistics of the noise signal.

Chapter 3

Assumed current distributions

Section 3.1 discusses the assumed current distribution that uses the Gaussian approximation of pdfs of the marks and the spaces at the decision point in the receiver. Section 3.2 discusses the assumed current distribution that uses the generalized χ^2 pdfs of the currents, which are exact for the receiver models that we are using. Section 3.3 describes the C++ algorithm to calculate the pdfs using these two current distribution models.

3.1 Gaussian current distribution

For an arbitrary optical field and additive white Gaussian noise (AWGN) at the input of the receiver with arbitrary optical and electrical filter shapes, Winzer [11] derived the first two central moments of the filtered electric current in the marks and spaces. I will now describe the mathematical procedure. The notation and discussion follows Lima [17].

Let us designate the optical field incorporating all propagation influences

at the input of the receiver as $e_{\text{in}}(t)$. We assume that the optical noise from the in-line EDFAs in the transmission line is the dominant source of noise in the system and that this noise $n(t)$ at the input of the receiver is AWGN. Let N_{ASE} be the noise power spectral density. The receiver consists of an optical filter with a transfer function $H_o(\omega)$ and with an impulse response $h_o(t)$, a photodetector that is mathematically modeled as a square-law device having responsivity κ , and an electric filter with a transfer function $H_e(\omega)$ and with an impulse response $h_e(t)$. The filters are modeled as lossless devices, *i.e.*, the area of the impulse response functions is unity, so that $H(0) = \int_{-\infty}^{\infty} h(t)dt = 1$. The filtered current at the output of the electric filter is given by

$$i = \kappa \left\{ \left| \left[e_{\text{in}} + n \right] * h_o \right|^2 * h_e \right\}, \quad (3.1)$$

where the convolution of two functions A and B of time t is defined by $(A * B)(t) = \int_{-\infty}^{\infty} A(\tau)B(t - \tau)d\tau$. The noiseless current at clock recovery time t_{clk} is given by $i(t_{\text{clk}})$. The clock recovery time is found numerically by using the 10 GHz tone of the optical signal.

The noise current is given by

$$i_n = \kappa \left[\left| n * h_o \right|^2 * h_e \right]. \quad (3.2)$$

The mean current due to noise is a constant and given by $\langle i_n \rangle(t) = \langle i_n \rangle = N_{\text{ASE}}B_o$, where B_o is the power spectral bandwidth of the optical filter. The mean current at clock recovery time is the sum of the noiseless electric current at the clock recovery time $i(t_{\text{clk}})$ and the mean noise current $\langle i_n \rangle$.

The variance of the electric filtered current is given by

$$\sigma^2(t) = \langle i^2 \rangle(t) - \langle i \rangle^2(t) = \sigma_{\text{ASE-ASE}}^2 + \sigma_{\text{S-ASE}}^2(t), \quad (3.3)$$

where $\sigma_{\text{ASE-ASE}}^2$ is the variance in current due to noise-noise beating in the receiver and $\sigma_{\text{S-ASE}}^2$ is the variance in the current due to signal-noise beating. The value of $\sigma_{\text{ASE-ASE}}^2$ is given by

$$\sigma_{\text{ASE-ASE}}^2 = N_{\text{ASE}}^2 \kappa^2 \int_{-\infty}^{\infty} |r_o(\tau)|^2 r_e(\tau) d\tau, \quad (3.4)$$

where $r_o(\tau) = \int_{-\infty}^{\infty} h_0(\tau') h_0^*(\tau + \tau') d\tau'$ and $r_e(\tau) = \int_{-\infty}^{\infty} h_e(\tau') h_e^*(\tau + \tau') d\tau'$ are the autocorrelation functions of the optical and the electrical filters, respectively.

The variance due to signal-noise beating can be written as

$$\sigma_{\text{S-ASE}}^2(t) = N_{\text{ASE}}^2 \kappa^2 \int_{-\infty}^{\infty} e_{\text{out}}(\tau) h_e(t-\tau) d\tau \times \int_{-\infty}^{\infty} e_{\text{out}}^*(\tau') h_e(t-\tau') r_o(t-\tau') d\tau', \quad (3.5)$$

where $e_{\text{out}} = e_{\text{in}} * h_o$. The variance of the current is also computed at the clock recovery time.

Hence, the first two central moments of the current in the marks and spaces can be computed. Since the Gaussian distribution is completely specified by the first two central moments, there is now sufficient information to approximate the pdfs of the current in each bit by Gaussian functions. The pdfs of the currents in all the transmitted marks is averaged to yield the average pdf of the current in the marks. A similar procedure is used to obtain the average pdf of the current in the spaces. The BER as a function of decision

voltage can then be computed using Equation (2.14). The minimum BER and the corresponding value of decision threshold are thus obtained.

3.2 χ^2 current distribution

In this section, I describe the current distribution model that provides the generalized χ^2 pdfs of the electric current in the receiver. This model is based on the work of Holzlöhner, *et al.* [18]–[19].

Let $u_o(t)$ and $\delta u(t)$ represent the noiseless optical field and the total accumulated noise field at the input of the receiver, respectively. We express $u_o(t)$ and $\delta u(t)$ as a Fourier series,

$$u_o(t) = \sum_{l=-N/2}^{N/2-1} A_l \exp(-iw_l t), \quad (3.6a)$$

$$\delta u(t) = \sum_{l=-N/2}^{N/2-1} r_l \exp(-iw_l t), \quad (3.6b)$$

where $w_l = 2\pi l/T$ and T is the time period of the signal. A real signal is not periodic, but we may take T to be very large. We use this periodic analysis for computational convenience.

The effect of optical filtering is to multiply the Fourier components of the input noisy signal by the filter function $H^{\text{opt}}(\omega)$ in the frequency domain. Assuming that the photodetector is an ideal square law detector with responsivity κ , we obtain

$$I(t) = \kappa \sum_{k=-N/2}^{N/2-1} \sum_{l=-N/2}^{N/2-1} (A_k + r_k)^* H_k^{\text{opt}*} (A_l + r_l) H_l^{\text{opt}} \exp[-it(\omega_l - \omega_k)], \quad (3.7)$$

where z^* denotes the complex conjugate of z . The filtered current $y(t)$ after passing the current $I(t)$ through a low pass electrical filter is given by

$$y(t) = \kappa \sum_{k=-N/2}^{N/2-1} \sum_{l=-N/2}^{N/2-1} (A_k + r_k)^* H_k^{\text{opt}*} (A_l + r_l) H_l^{\text{opt}} \exp[-it(\omega_l - \omega_k)] H_{l-k}^{\text{el}}. \quad (3.8)$$

We define a complex matrix \mathbf{W} of size $N \times N$,

$$\mathbf{W}_{kl}(t) = \kappa H_k^{\text{opt}*} H_l^{\text{opt}} H_{l-k}^{\text{el}} \exp(-it\omega_{l-k}), \quad (3.9)$$

that takes into account the combined effect of the optical filter, the photodetector, and the electrical filter. We may now write $y(t)$ as

$$y(t) = \kappa \sum_{k,l=-N/2}^{N/2-1} (A_k + r_k)^* \mathbf{W}_{kl}(t) (A_l + r_l). \quad (3.10)$$

Since y is real for all t , \mathbf{W} must be a Hermitian matrix, so that $\mathbf{W}_{kl}(t) = \mathbf{W}_{lk}^*(t)$. I next express the complex Fourier coefficients A_k of the signal $u_0(t)$ as a real vector, $\mathbf{A} = (A_{-N/2,R}, \dots, A_{N/2-1,R}, A_{-N/2,I}, \dots, A_{N/2-1,I})^T$, where the subscripts R and I refer to the real and imaginary parts of each component. We similarly express the components r_k of the noise $\delta u(t)$ as a real vector $\mathbf{r} = (r_{-N/2,R}, \dots, r_{N/2-1,R}, r_{-N/2,I}, \dots, r_{N/2-1,I})^T$.

We may now re-express $y(t)$ and \mathbf{W} ,

$$y(t) = (\mathbf{A} + \mathbf{r})^T \mathcal{W}(t) (\mathbf{A} + \mathbf{r}), \quad (3.11a)$$

$$\mathcal{W} = \begin{bmatrix} \mathbf{W}_R & -\mathbf{W}_I \\ \mathbf{W}_I & \mathbf{W}_R \end{bmatrix} = \mathcal{W}^T, \quad (3.11b)$$

where W_R is the real part of W and W_I is the imaginary part of W .

To derive the pdf of the current $y(t)$, we first find the Karhunen-Loève modes of $y(t)$, thereby expressing $y(t)$ as a sum of independent random variables. The convolution of the pdfs of these random variables then determines the pdf of the current.

In Subsection 2.3.3 I showed that the noise covariance matrix is a diagonal matrix when the noise is white. Hence, both the filter matrix \mathcal{W} and the inverse noise covariance matrix \mathcal{K}^{-1} are symmetric matrices and positive definite, so that they may be simultaneously diagonalized. By doing so, we manage to introduce the noise moments into the equation of the filtered current. Next we apply the theory of simultaneous diagonalization [20], which states that there exists a real matrix C satisfying

$$\mathcal{K}^{-1} = C^T C, \quad (3.12a)$$

$$\mathcal{W} = C^T \Lambda C, \quad (3.12b)$$

where Λ is a time-independent diagonal matrix in which each element λ_k is real. In the case presented here in which one considers additive white Gaussian noise at the receiver without transmission effects, the covariance matrix \mathcal{K} becomes an identity matrix multiplied by a scalar. The problem of simultaneous diagonalization then reduces to a simple diagonalization. The transformation C yields the Karhunen-Loève modes of y . From (3.11a) and

(3.12b) we find,

$$\begin{aligned} y(t) &= (\mathbf{A} + r)^T C^T \Lambda C (\mathbf{A} + r), \\ y(t) &= (\mathbf{Q} + \mathbf{q})^T \Lambda (\mathbf{Q} + \mathbf{q}), \end{aligned} \quad (3.13)$$

where $Q_k(t) \equiv C_{kl}(t)A_l$ represents the Karhunen-Loève modes of the noise-free signal and $q_k(t) \equiv C_{kl}(t)r_l$ represents the noise modes. Expanding $y(t)$, we obtain

$$y(t) = \sum_{k=1}^{2N} \lambda_k (Q_k^2 + 2Q_k q_k + q_k^2) = \sum_{k=1}^{2N} g_k, \quad (3.14)$$

where $g_k \equiv \lambda_k (Q_k^2 + 2Q_k q_k + q_k^2)$ represents a set of independent random variables. Since $y(t)$ can be written as a sum of independent random variables, its pdf $p_y(t)$ is a convolution of the pdfs of these random variables,

$$p_y(y, t) = p_{g1}(g_1, t) * p_{g2}(g_2, t) \cdots * p_{g2N}(g_{2N}, t). \quad (3.15)$$

We next exploit the Fourier transform property that convolution in one domain is multiplication in the other domain. Hence, this convolution may be transformed into simple multiplications of characteristic functions. The characteristic function and the pdf of a random variable h are related to each other by the Fourier transform, so that,

$$\Phi_h(\zeta) = \int_{-\infty}^{\infty} \exp(i\zeta h) p_h dh, \quad (3.16a)$$

$$p_h = \frac{1}{2\pi} \int_{-\infty}^{\infty} \exp(-i\zeta h) \phi(\zeta) d\zeta. \quad (3.16b)$$

To obtain the characteristic function of $g_k(t)$, we first note that the pdf of

any noise mode p_{qk} is Gaussian with zero mean and unit variance. The variance is unity because the covariance matrix is an identity matrix, so that $p_{qk}(q_k) \equiv \exp(-q_k^2/2)/\sqrt{2\pi}$. Therefore, the characteristic function of g_k , Φ_{gk} is

$$\begin{aligned}\Phi_{gk}(\zeta) &= \int_{-\infty}^{\infty} \exp[i\zeta g_k] p_{gk} dg_k \\ &= \frac{1}{\sqrt{2\pi}} \int_{-\infty}^{\infty} \exp\left[-\frac{q_k^2}{2} + i\zeta \lambda_k (Q_k^2 + 2Q_k q_k + q_k^2)\right] dq_k.\end{aligned}\quad (3.17)$$

By making a change of variables, we can convert (3.17) into a complete gamma function. It can be shown that

$$\Phi_{gk}(\zeta) = \frac{1}{\sqrt{1 - 2i\lambda_k\zeta}} \exp\left(\frac{i\lambda_k Q_k^2 \zeta}{1 - 2i\lambda_k\zeta}\right).\quad (3.18)$$

The characteristic function of y , $\Phi_y(\zeta, t)$ equals the product of the Φ_{gk} .

$$\begin{aligned}\Phi_y(\zeta, t) &= \prod_{k=1}^{2N} \Phi_{gk}, \\ &= \left(\prod_{k=1}^{2N} \frac{1}{\sqrt{1 - 2i\lambda_k\zeta}}\right) \exp\left(i\zeta \sum_{k=1}^{2N} \frac{\lambda_k Q_k^2}{1 - 2i\lambda_k\zeta}\right).\end{aligned}\quad (3.19)$$

The pdf p_y can now be obtained by taking the Fourier transform of equation (3.19), so that

$$p_y(y, t) = \frac{1}{2\pi} \int_{-\infty}^{\infty} \exp(-i\zeta y) \phi_y(\zeta, t) d\zeta.\quad (3.20)$$

One may attempt to evaluate (3.20) numerically by using a discrete Fourier transform. However, this approach is impaired by round-off errors in numer-

ical computation at low values of the pdf ($< 10^{-10}$). A better approach is to utilize the steepest descent method [3]. Essentially, we convert the real integral in equation (3.20) to a contour integral in the complex plane by making a change of variables from ζ to s , where, $s = i\zeta$. It is then possible to write the integral in equation (3.20) as

$$p_y(y, t) = \frac{1}{2\pi i} \int_C \exp[\psi(s, y)] ds. \quad (3.21)$$

where C is the contour path of integration. It can be shown that ψ is analytical over the complex plane except at certain points on the real number line that correspond to $1/(2\lambda_k)$. The contour of integration corresponds to the curve on which $\text{Im}(\psi)$ is constant, corresponding to the path of steepest descent or ascent for $\text{Re}(\psi)$. It can also be shown that most of the contribution to the integral in (3.21) is from a small part of the contour around the saddle point and hence we can roughly approximate $\psi(s)$ around the saddle point by considering only the first few terms of its Taylor series. The saddle point of ψ can be found numerically for each value of current and each instance of time, and the final pdf has the form

$$p_y(y, t) = \frac{1}{\sqrt{2\pi\psi''[u(y)]}} \exp\{\psi[u(y)]\}, \quad (3.22)$$

where $u(y)$ is the saddle point, which is computed numerically.

For every bit in the transmitted signal, $p_y(y)$ is found numerically at the clock recovery time. The pdfs of the current in the marks and spaces are then summed and averaged. From these curves of the average pdfs, the BER

is computed numerically. The first two central moments of the pdfs of the current in each individual bit are also found and the Gaussian-approximated pdfs can then be found from these moments.

3.3 Algorithm

The computation of the pdfs and the BER of the electrical current in the receiver has been implemented in C++. I will describe the main steps in the computation of the pdfs in this section.

1. Read in the noiseless optical signal A , the filter functions and their bandwidths, and the OSNR value.
2. Compute the signal power. The noise power and noise spectral density are then found. The elements on the diagonal elements of the covariance matrix \mathcal{K}_{ii} are directly proportional to the noise spectral density.
3. Compute the time independent part of the filter matrix W .
4. Find the clock recovery time using the carrier tone in the optical signal.
5. Build a time vector comprised of the sampling times in each bit.
6. Start a loop over all points in the time vector, for which the pdf is to be computed.
 - (a) Compute the Hermitian matrix $W_{kl}(t)$.
 - (b) Compute C and Λ by solving the eigenvalue problem in (3.12a) and (3.12b).

- (c) Start another loop over all points in the electrical current vector.
 - i. Find the saddle point of the function ψ in (3.21).
 - ii. For every instant of time and for every current value, the pdf is found using (3.22).
 - (d) Find the first two central moments in each bit and use them to generate Gaussian pdfs.
7. Average the pdfs of the marks and spaces and compute the BER for all values in the decision threshold vector. Find the minimum BER and the corresponding decision threshold.
8. As in 7, find the minimum BER and the corresponding decision threshold when the Gaussian approximation of the current pdf is used.

Chapter 4

Results

In this chapter, I present the results of comparing the integrate-and-dump receiver model consisting of an optical bandpass filter, a square law detector and an integrate-and-dump electrical filter with a realistic receiver model consisting of a three-mirror Fabry-Perot filter, a photodetector, and a fifth-order Bessel filter. My colleagues and I compared the BERs and the corresponding decision thresholds for the two receiver models, using two assumed current distribution — the χ^2 current distribution and the Gaussian current distribution.

We performed the comparisons of the two receiver models over an extensive set of system parameters. The elements of this parameter set include optical and electrical filter bandwidths, signal and noise power levels, signal modulation format (RZ and NRZ), extinction ratio in the spaces of the signal, rise time of NRZ pulses and pulsewidth of RZ pulses. The comparison between the two receiver models is achieved by looking at the impact of changing the variables in the parameter set just described above and evaluating the

BER produced by the two receiver models.

The simulation results are shown for a 10 Gb/s single-channel system. To account for all 3-bit pattern dependencies in the receiver an 8-bit pulse sequence 11101000 is transmitted, which is a de Bruijn sequence containing all 3-bit combinations of zeros and ones.

4.1 Effect of varying electrical filter bandwidth

RZ pulse format

An RZ modulation format pulse sequence, with peak power 1 mW and 33 ps pulse duration is transmitted. The extinction ratio in the spaces of the transmitted signal is 20 dB. The noise energy due to the optical pre-amplifier is set so that the OSNR at the receiver input is 15 dB. For the realistic receiver model, we kept the bandwidth of the Fabry-Perot filter fixed, and we varied the 3-dB bandwidth of the Bessel filter over a range from 4–12 GHz. For the integrate-and-dump receiver model, we choose the bandwidth of the rectangular optical filter is chosen such that it is equivalent to the B_o bandwidth of the Fabry-Perot filter. A 3-mirror Fabry-Perot filter having a FWHM bandwidth of 50 GHz has an equivalent B_o bandwidth of 55.46 GHz. The bandwidth of the integrate-and-dump filter depends on the integration time, which equals the bit period. Hence, if the bit period is constant, then the integrate-and-dump filter bandwidth remains constant. In Fig. 4.1 and Fig. 4.2, for the integrate-and-dump receiver, the BER and decision voltage curves are shown as constant functions. These straight lines correspond to a single data point, as the bandwidth of the integrate-and-dump filter is a

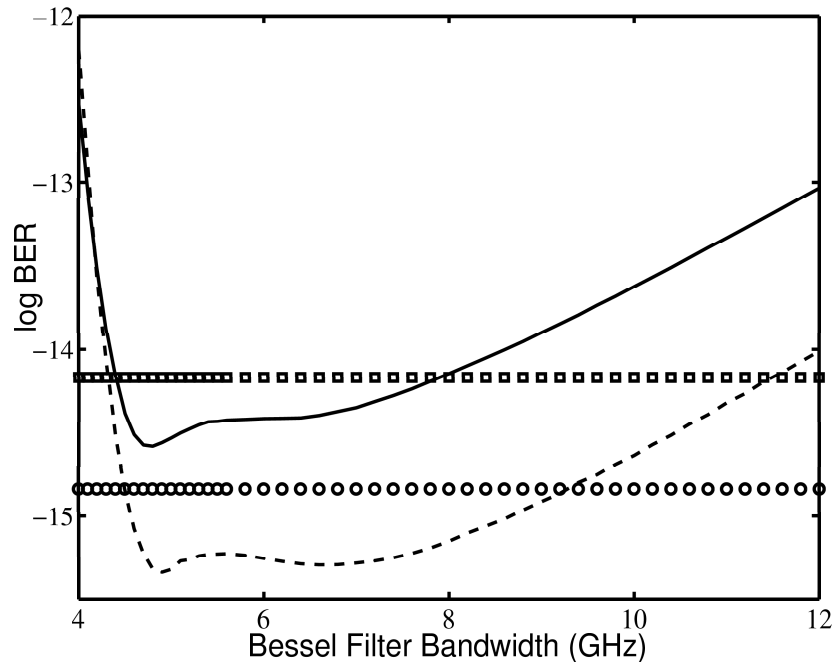


Figure 4.1: RZ pulse format. BER as a function of the electrical filter bandwidth. The BER variations for a realistic receiver model using a Gaussian current distribution and a χ^2 current distribution are shown by dashed and solid curves, respectively. The results for the integrate-and-dump receiver model using a Gaussian current distribution and a χ^2 current distribution are shown by straight lines, marked by circles and squares respectively.

constant.

In Fig. 4.1, one finds for Bessel filter bandwidths ≤ 5 GHz that the BER is large for the realistic receiver model. This BER is large because the pulses in the noiseless filtered signal are highly distorted, so that a significant amount of inter-symbol interference (ISI) is present. For filter bandwidths ≥ 8 GHz, we find that as one increases the filter bandwidth, more noise is allowed to pass through the filter, which results in higher values of BER. In the bandwidth region between 5 GHz and 8 GHz, there is a trade off between ISI effects and noise effects. The region between 5 GHz and 8 GHz is the optimum

bandwidth region.

In the optimum bandwidth region between 5 GHz and 8 GHz, the difference in BER between the realistic receiver model using a χ^2 current distribution and the integrate-and-dump receiver model using either of the two current distributions is about half an order of magnitude.

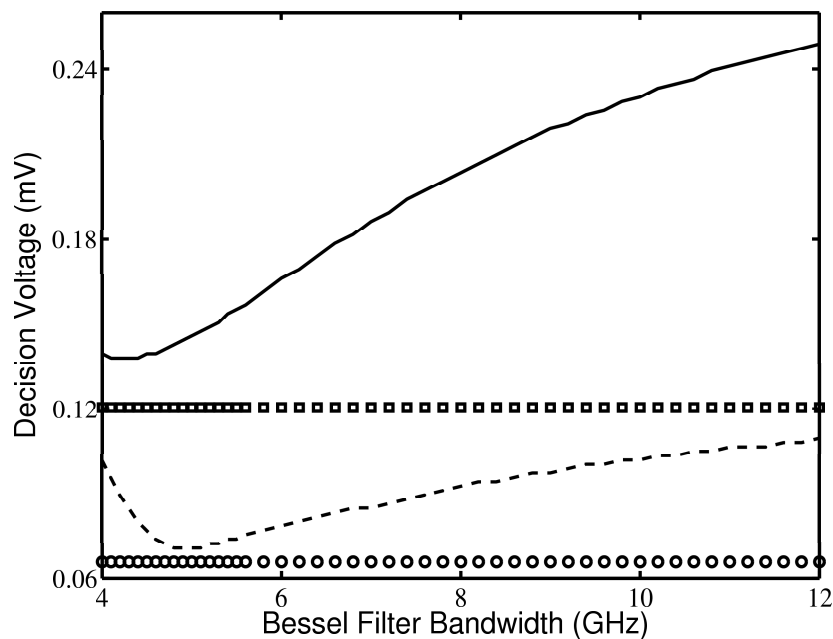


Figure 4.2: RZ pulse format. Decision threshold as a function of the electrical filter bandwidth. The decision threshold variations for a realistic receiver model using a Gaussian current distribution and a χ^2 current distribution are shown by dashed and solid curves, respectively. The results for the integrate-and-dump receiver model using a Gaussian current distribution and a χ^2 current distribution are shown by straight lines, marked by circles and squares respectively.

In the bandwidth region between 5 GHz and 8 GHz, the decision voltage difference between the realistic receiver model and the integrate-and-dump receiver model with a χ^2 current distribution varies from 2% to 8% of the peak signal power at the transmitter. The difference between the realistic

receiver model using a χ^2 current distribution and the integrate-and-dump receiver model using a Gaussian current distribution is significantly more and is in the range of 8% to 14% of the peak signal power at the transmitter.

NRZ pulse format

An NRZ modulation format pulse sequence is transmitted with a rise time of 30 ps and an average power which is the same as that of an RZ pulse with 1 mW peak power and 33 ps pulse duration. The extinction ratio in the spaces of the transmitted signal is set to 20 dB, and the OSNR at the receiver input is set to 15 dB.

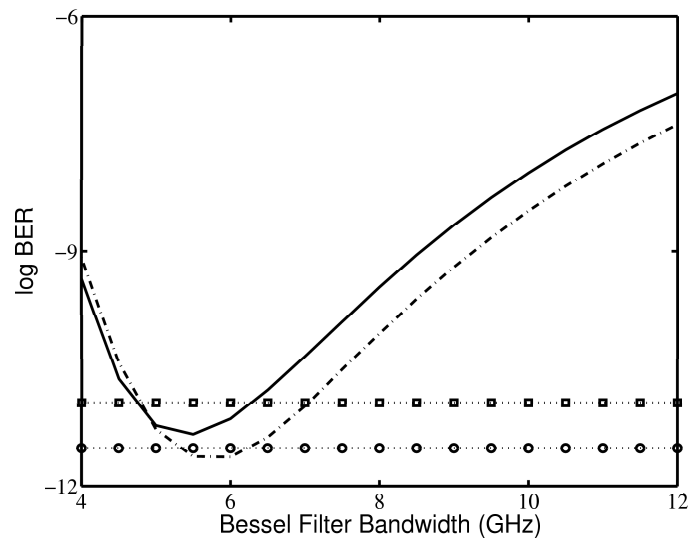


Figure 4.3: NRZ pulse format. BER as a function of the electrical filter bandwidth. The BER variations for a realistic receiver model using a Gaussian current distribution and a χ^2 current distribution are shown by dashed and solid curves, respectively. The results for the integrate-and-dump receiver model using a Gaussian current distribution and a χ^2 current distribution are shown by straight lines, marked by circles and squares respectively.

In Fig. 4.3, the behavior of the BER curves as a function of filter band-

width for the realistic receiver model can be attributed to ISI effects that are dominant at bandwidths less than 4.5 GHz and noise at bandwidths greater than 6.5 GHz. Since the NRZ signal has a smaller bandwidth than does the RZ signal, the optimum threshold level is reached earlier and the optimum filter bandwidth region is much shorter. From Figs 4.1 and 4.3, we find that the RZ modulation format yields significantly lower BERs than does the NRZ format.

In the optimum bandwidth region between 4.5 GHz and 6.5 GHz, the difference in BER between the realistic receiver model using a χ^2 current distribution and the integrate-and-dump receiver model using either of the two current distributions is about three-tenths of an order of magnitude.

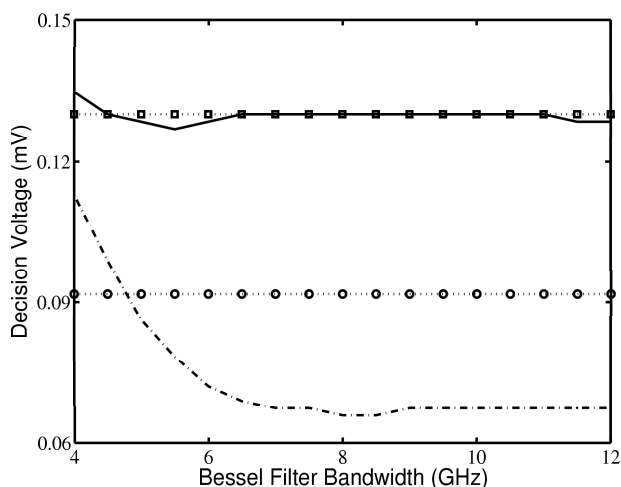


Figure 4.4: Decision threshold as a function of the electrical filter bandwidth for the NRZ pulse format. The decision threshold variations for a realistic receiver model using a Gaussian current distribution and a χ^2 current distribution are shown by dashed and solid curves, respectively. The results for the integrate-and-dump receiver model using a Gaussian current distribution and a χ^2 current distribution are shown by straight lines, marked by circles and squares respectively.

In Fig. 4.4, there is little difference between the decision thresholds that we obtain with the integrate-and-dump receiver model and the realistic receiver model using a χ^2 current distribution. The difference in the decision voltage between the integrate-and-dump receiver model using a Gaussian current distribution and a realistic receiver model using a χ^2 current distribution is about 4% of the transmitted signal peak power.

4.2 Effect of varying signal rise time

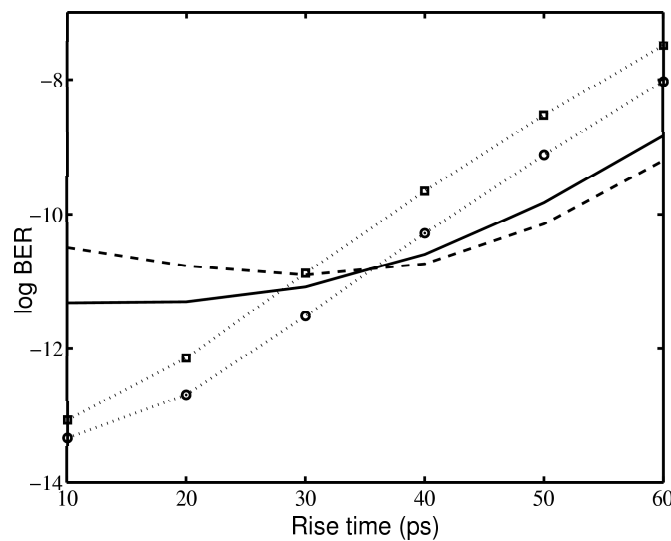


Figure 4.5: Variation of the BER with a change in rise time of the NRZ pulse. The results for the realistic receiver model using a Gaussian current distribution and a χ^2 current distribution are shown by dashed and solid lines, respectively. The results for the integrate-and-dump receiver model using a Gaussian current distribution and a χ^2 current distribution are shown by the dotted lines, marked by circles and squares respectively.

In our simulations, NRZ pulses are produced from perfect rectangular pulses that are filtered by Gaussian shape filters. The rise time of the NRZ

pulse is a function of the Gaussian filter bandwidth. For an NRZ pulse, a larger rise time implies a smaller signal bandwidth.

The extinction ratio in the spaces of the transmitted signal is set to 20 dB, and the OSNR at the receiver input is set to 15 dB. The bandwidths of the optical and electrical filter in the realistic receiver are set to 50 GHz (FWHM) and 6 GHz (3 dB bandwidth), respectively. In Fig. 4.5, as the rise time of the NRZ pulse increases, the signal bandwidth decreases and the signal power also decreases. As a consequence, the pdfs of the receiver current spread out, and the BER increases. There is a significant difference between the BER curves for the integrate-and-dump receiver model using a Gaussian current distribution model and the realistic receiver model using a χ^2 current distribution. In Fig. 4.6, the disparity between the decision voltage results for

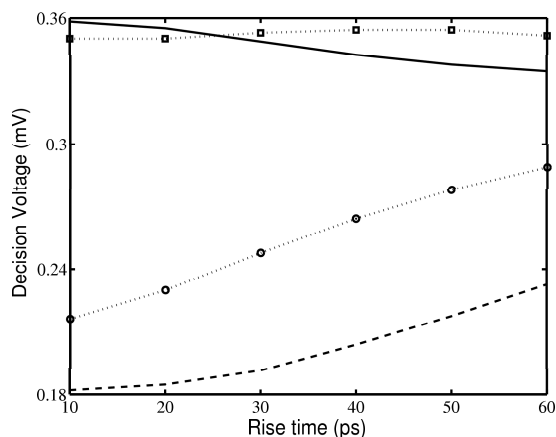


Figure 4.6: Variation of decision voltage with change in rise time of the NRZ pulse. The results for the realistic receiver model using a Gaussian current distribution and a χ^2 current distribution are shown by dashed and solid lines, respectively. The results for the integrate-and-dump receiver model using a Gaussian current distribution and a χ^2 current distribution are shown by the dotted lines, marked by circles and squares respectively.

the integrate-and-dump receiver model using a Gaussian current distribution and the realistic receiver model using a χ^2 current distribution is also large.

4.3 Effect of varying OSNR

An RZ modulation format pulse sequence, with a peak power of 1 mW and a 33 ps pulse duration is transmitted. The extinction ratio in the spaces of the transmitted signal is 20 dB. For the realistic receiver model, the optical filter FWHM is set to 50 GHz and the electrical filter 3-dB bandwidth is set to 8 GHz. The OSNR is varied by varying the noise power added by the pre-amplifier to the receiver. As the OSNR increases, the noise power decreases because the signal power is kept constant. Hence in Fig. 4.7, the BER decreases as OSNR increases. The difference between BERs for the

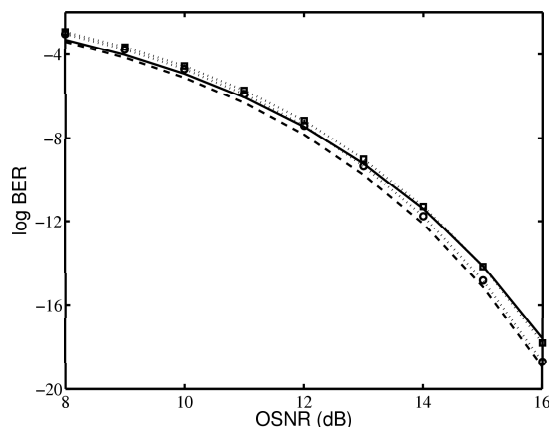


Figure 4.7: Variation of the BER versus OSNR for the RZ modulation format. The BER variations for the realistic receiver model using a Gaussian current distribution and a χ^2 current distribution are shown by dashed and solid curves, respectively. The results for the integrate-and-dump receiver model using a Gaussian current distribution and a χ^2 current distribution are shown by dotted lines, marked by circles and squares respectively.

realistic receiver model and the integrate-and-dump receiver model, using a χ^2 current distribution does not change significantly with OSNR. However, there is a visible difference between the BERs for the realistic receiver model using a χ^2 current distribution and the integrate-and-dump receiver model using a Gaussian current distribution. This difference increases as the noise power decreases and the OSNR increases.

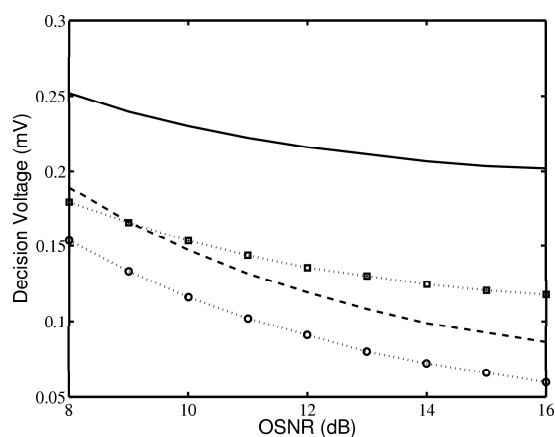


Figure 4.8: Variation of the decision voltage versus OSNR for the RZ modulation format. The decision threshold variations for the realistic receiver model using a Gaussian current distribution and a χ^2 current distribution are shown by dashed and solid curves, respectively. The results for the integrate-and-dump receiver model using a Gaussian current distribution and a χ^2 current distribution are shown by dotted lines, marked by circles and squares respectively.

Chapter 5

Conclusion

In this thesis, I present a performance comparison between an ideal receiver model and a realistic receiver model. In order to focus on the receiver, my colleagues and I have modeled the optical noise at the receiver input as AWGN and have not considered any transmission or inter-channel effects.

From the figures shown in Chapter 4, we conclude that over a broad set of system parameters, the performance of the two receiver models are comparable. A comparison between the integrate-and-dump receiver model and the realistic receiver model with a current distribution model using generalized χ^2 pdfs shows that the minimum BERs differ only by an order of magnitude. Hence, one may use the integrate-and-dump receiver model which may simplify the calculation of the current distribution in the receiver, without significantly degrading the accuracy of the BER results.

The comparison between the integrate-and-dump receiver model with a current distribution model employing a Gaussian approximation of the pdfs and the realistic receiver model with a current distribution model using gen-

eralized χ^2 pdfs shows that the minimum BERs differ by about one to two orders of magnitude. It has been shown in earlier work [4], [5] that the Gaussian approximation of pdfs of the current in the receiver overestimates the minimum BER by an order of magnitude. In our comparison, we observe the same.

Further work on this topic could potentially focus on the impact of using differential phase shift keyed (DPSK) modulation format and could consider inter-channel effects.

Bibliography

- [1] G. P. Agrawal, *Fiber-Optic Communication Systems*, Wiley, New York, 2nd edition, 1997.
- [2] J. S. Lee and C. S. Shim, “Bit-error-rate analysis of optically preamplified receivers using an eigenfunction expansion method in optical frequency domain,” *J. Lightwave Technol.*, vol. 12, pp. 1224–1229, 1994.
- [3] E. Forestieri, “Evaluating the error probability in lightwave systems with chromatic dispersion, arbitrary pulse shape and pre- and postdetection filtering,” *J. Lightwave Technol.*, vol. 18, pp. 1493–1503, 2000.
- [4] D. Marcuse, “Derivation of analytical expressions for the bit-error probability in lightwave systems with optical amplifiers,” *J. Lightwave Technol.*, vol. 8, pp. 1816–1823, 1990.
- [5] P. A. Humblet and M. Azizoglu, “On the bit error rate of lightwave systems with optical amplifiers,” *J. Lightwave Technol.*, vol. 9, pp. 1576–1582, 1991.
- [6] A. Kalra, J. Zweck, and C. R. Menyuk, “Comparison of bit-error ratios for receiver models with integrate-and-dump and realistic electrical filters

- using the Gaussian approximation,” in *Proc. Conf. Lasers and Electro-Optics*, San Francisco, CA, 2004, paper CWA24.
- [7] E. Desurvire, *Erbium-Doped Fiber Amplifiers: Principles and Applications*, Wiley, New York, 1994.
- [8] R. Y. Rubenstein, *Simulation and the Monte Carlo Method*, Wiley, New York, 1st edition, 1981.
- [9] I. P. Kaminov and T. L. Koch, *Optical Fiber Telecommunications IIIA*, Academic Press, San Diego, 1997.
- [10] H. Jiao, I. T. Lima Jr., A. O. Lima, Y. Sun, J. Zweck, L. Yan, C. R. Menyuk, and G. M. Carter, “Experimental validation of an accurate receiver model for systems with unpolarized noise,” in *Proc. Conf. Lasers and Electro-Optics*, Baltimore, MD, 2003, paper CThJ1.
- [11] P. J. Winzer, M. Pfennigbauer, M. M. Strasser, and W. R. Leeb, “Optimum filter bandwidths for optically preamplified NRZ receivers,” *J. Lightwave Technol.*, vol. 19, pp. 1263–1273, 2001.
- [12] Mário M. Freire, Álvaro M. F. de Carvalho, and Henrique J. A. da Silva, “Performance implications of three-mirror Fabry-Perot demultiplexers for 10Gb/s WDM dispersion-supported transmission with 0.5-nm channel spacing,” *IEEE Photon. Technol. Lett.*, vol. 8, pp. 1261–1263, 1996.
- [13] J. Stone, L. W. Stulz, and A. A. M. Saleh, “Three-mirror fiber Fabry-Perot filters of optimal design,” *Electron. Lett.*, vol. 26, pp. 1073–1074, 1990.

- [14] R. Schaumann and Valkenburg M. E. Van, *Design of Analog Filters*, Oxford University Press, 2nd edition, 2001.
- [15] H. Heffner, “The fundamental limit of linear amplifiers,” in *Proc. IRE*, 1962, vol. 50, pp. 1604–1608.
- [16] L. G. Kazovsky, S. Benedetto, and Willner A. E., *Optical Fiber Communication Systems*, Artech House, Norwood, MA, 1996.
- [17] I. T. Lima Jr., A. O. Lima, J. Zweck, and C. R. Menyuk, “Performance characterization of chirped return-to-zero modulation format using an accurate receiver model,” *IEEE Photon. Technol. Lett.*, vol. 15, pp. 608–610, 2003.
- [18] R. Holzlohner, V. S. Grigoryan, C. R. Menyuk, and W. L. Kath, “Accurate calculation of eye diagrams and bit error rates in optical transmission systems using linearization,” *J. Lightwave Technol.*, vol. 20, pp. 389–400, 2002.
- [19] R. Holzlohner, C. R. Menyuk, W. L. Kath, and V. S. Grigoryan, “A covariance matrix method to compute accurate bit error rates in a highly nonlinear dispersion-managed soliton system,” *Photon. Technol. Lett.*, vol. 15, pp. 688–690, 2003.
- [20] J. Franklin, *Matrix Theory*, Prentice-Hall, New Jersey, 1968.